Vegetation monitoring via a novel push-broom-sensor-based hyperspectral device

IOP Conf. Series: Journal of Physics: Conf. Series **1249** (2019) 012007 doi:10.1088/1742-6596/1249/1/012007

Vegetation monitoring via a novel push-broom-sensor-based hyperspectral device

Monica Moroni

DICEA-Sapienza University of Rome, via Eudossiana 18, 00184 Rome, Italy

monica.moroni@uniroma1.it

Abstract. Due to their remarkable spatial and spectral resolution, hyperspectral sensing devices appear the most suited for detection of vegetation presence according to the peculiar spectral features that vegetation exhibits. Among the applications, vegetation identification as well as vegetation health-state detection via spectral data analysis is feasible due to the modifications the typical vegetation spectral signature undergoes when abnormalities are present. A push-broom-sensor-based spectral device characterized by low cost, weight, power consumption, and no need of GPS/inertial measurement units for post- flight georeferencing was placed on an airplane and employed for the acquisition of spectral data in a wide territory. The proximal sensing field campaign was carried out in San Teodoro (Olbia-Tempio-Sardinia). Classification procedures and the employment of vegetation indices made it possible to identify the vegetated areas. The platform characteristics and the methodology developed allow vegetation to be investigated within a large interval of scales from a few centimeters to some hundred meters. Data acquired agree well with thematic maps of the areas under investigation. The broadband indices Red DVI, SR and TVI perform remarkably well in highlighting the presence of vegetation.

1. Introduction

The huge potentiality of vegetation monitoring via the analysis of hyperspectral data is largely documented in the literature with interesting applications aimed at identifying different plants and the eventual start and evolution of stress situations [1-3].

It is well-known that healthy plants present unique spectral properties strictly connected to their chemical composition (pigments and other biochemical constituents), the physical (leaf thickness, mesophyll structure) and physiological (water content, photosynthetic efficiency) characteristics of the leaf apparatus [4]. Airborne hyperspectral sensing systems supply high spatial, spectral and temporal resolution data and are for this reason particularly suited for vegetation monitoring [5-6]. One of the most relevant applications is in the context of the quantitative estimate of biochemical and biophysical variables related to the physiological state of vegetation and of the occurrence of stress situations. The timely identification of stress situations is particularly relevant to facilitate the identification of targeted areas and the design of localized actions that limit costs and avoid degradation of the environment with unnecessary treatments (anticrittogamics, insecticides) [7]. To handle the huge amount of information provided by hyperspectral sensing systems, it is useful to compute proper hyperspectral indices that synthesize reflectance characteristics. The indices, which in the case of vegetation monitoring are called vegetation indices, VIs, are in most of the cases functions of the reflectance in red (R) and near-infrared (NIR) spectral bands [8]. Vegetation indices are empirically determined combinations of bands

associated to the specific features of the vegetation spectral signatures. [9] and [10] presented a useful and complete review of vegetation indices available in the literature discussing their specific applicability and representativeness according to the vegetation of interest, environment, and implementation precision. In field applications, optimal VIs are usually tailored to the specific application requirements coupled with appropriate validation tools and methodologies in the ground [11].

VIs have been widely implemented within remote sensing applications using different airborne and satellite platforms with recent advances using Unmanned Aerial Vehicles (UAV). [2] employed a micro-hyperspectral imager to study the temporal patterns of canopy fluorescence and reflectance indices related to physiology and canopy structure. [12] presented vegetation map created by a UAS-based device and demonstrates that it could clearly discriminate community distributions being of particular usefulness where field reconnaissance is difficult. [13] presented UAS remote sensing for vegetation mapping in complex urban landscapes due to the ultra-high-resolution imagery acquired at low altitudes. [14] employed a small, fixed-wing UAS to survey a plot field experiment designed to estimate sorghum damage caused by an invasive aphid. Normalized difference vegetation index (NDVI) maps were built and correlated to aphid density.

In spite of the recent progresses documented by the literature, the design and development of hyperspectral manned or unmanned aircraft devices, as well as procedures for calibration, processing and interpretation of data collected are challenging tasks that require further developments [15]. Within this framework, the paper focuses on original procedures to process images acquired with a push-broom hyperspectral device designed and developed at the Department of Civil and Environmental Engineering of the Sapienza University of Rome. The spectrometer platform was realized by assembling commercial devices. It presents the following unique characteristics that make it suitable to be employed for monitoring actions in proximal sensing: (1) high spectral resolution (up to 3 nm in the wavelength interval 400-1800 nm); (2) high spatial resolution (on the order of centimeters); (3) easy portability, the system has been engineered so that it can be transported by manned or unmanned aircraft devices; (4) less costs, being a GPS/inertial measurement unit (IMU) unnecessary. An assembled platform was preferred to commercial spectral devices to reduce the investment costs and to control the weight of the equipment. However, algorithms for calibration, mosaicing, post-flight georeferencing and orthorectification of the acquired images had to be developed.

The above-mentioned platform was employed in a proximal sensing field campaign carried out in San Teodoro (Olbia-Tempio-Sardinia). To this aim, the spectrometer platform was mounted on an ultralight airplane. The purposes of the investigation were i) to develop the procedure for combining information contained in multiple, overlapping images of the same scene to produce a single image representing the entire investigated area and transfer to a push broom type spectral imaging and ii) to demonstrate the suitability of vegetation indices to identify vegetated areas.

This paper is organized as follows: Section 2 describes the push-broom hyperspectral device. Section 3 describes the algorithm for image mosaicing and post-flight georeferencing. Section 4 describes the results of the analysis of data acquired during the proximal sensing field campaign conducted in San Teodoro (Olbia-Tempio—Sardinia). The paper ends with a concluding section.

2. The hyperspectral sensor platform

The linear spectrometer Specim ImSpector VIS V10 OEM allows the acquisition of the hyperspectral information in the visible range of the electromagnetic spectrum (400 nm to 1000 nm). Through a slit, the spectrometer captures a line image of the target and disperses the light from each line image pixel into a spectrum. A Dalsa Falcon 1.4M100 CMOS camera (hereinafter spectrometer camera) of 1400×1024 pixel resolution (100 frames per second (fps) maximum acquisition frequency), is coupled to the spectrometer in order to acquire spectral images. Each spectral image contains the line pixels in a spatial axis and spectral pixels in a spectral axis (2D information). Spectral features of the entire target (3D information) can be obtained by acquiring images of the target while it is moving or by moving the spectral device. In the latter case, the position and altitude of the spectrometer camera must be precisely

recorded at the time of every frame capture for post- flight georeferencing. This is usually achieved by using GPS/IMUs. The time resolution of the IMU system must fit the frame rate employed for image acquisition and the procedure accuracy relies on highly accurate time stamping on images. Our system makes it possible to overcome the need of high time resolution IMU because post-flight georeferencing is performed employing a Dalsa 4M60 camera (hereinafter mosaicing camera) of 2352×1728 pixel resolution equipped with a standard lens. The spectrometer and mosaicing cameras are synchronized and arranged with parallel optical axes (acquisition frequency set to 25 fps). Each image acquired with the mosaicing camera will present only a portion of the target while each image acquired with the spectrometer camera will contain the spectral features of the target linear sub-portion seen through the slit. A mosaicing procedure is required to reconstruct the entire target and to properly georeference the line image acquired with the spectrometer camera.

The system for image storage consists of an IO Industries DVR Express ® Core provided with two camera link inputs. It is suitable to manage the transfer of 780 Mbytes/s. The device memory consists of four solid state disks for a total capacity of 1 Tbyte. The trigger signal that synchronizes the acquisition of the two cameras is generated by the Core. The device allows the acquisition and storage of images without any compression. A laptop manages the synchronization, acquisition and storage operations. The platform has been designed ensuring a reduced weight (less than 8 Kg) and low consumption (300 W at the start-up). Fig. 1 shows a picture of the ultralight airplane employed for the measurement campaign.

Figure 1. Ultralight airplane employed for the measurement campaign conducted in San Teodoro (Olbia-Tempio - Sardinia) using the spectrometer platform.

3. Spectral image processing procedures

Mosaicing is the procedure aimed at putting together several partially superimposed images to obtain only one image of the scene [16]. Three steps are mandatory to mosaic images: image registration, image reprojection, and image blending. The procedure for image registration requires an accurate point-to-point correspondence between images within the input sequence, i.e., given two consecutive images of the sequence, image points in the second image that correspond to the same points in the first image have to be found. Here we employ a methodology based on the correlation between consecutive images. This methodology is suitable to process the large number of images detected by an aircraft where it is assumed that no tilt occurs and that scale changes are the same in the two principal directions. The computation of the two-dimensional correlation between couples of consecutive images is based on the use of the two-dimensional Fourier transform (2-DFFT). Recalling that the rigid translation of an image with respect to the other one is related to the position of the peak of the 2-DFFT, the registration of the

i-th image on the scene is performed through iteratively applying the 2-DFFT procedure to each image pair. To take into account eventual rotations around the camera axis and variations in the distance between the point of view and the scene, the i-th image of the pair is rotated in the range of −5° to 5° with a 0.05° step, and the scale is modified relative to the original size of −6% to 6% with a step of 0.5%. The variation of scale, rotation and displacement that maximizes the consistency of the luminosity between the images of the pair is found. As a matter of fact, the procedure adopted is equivalent to a four-parameter homographic transformation (similarity). The implemented image blending function uses a simple averaging of intensity values. This is so because the main objective of the mosaicing procedure is to reproject the line acquired with the spectrometer. Mosaic rendering is not the objective of the procedure provided the mosaic is clear enough to comprehend the features of the area under investigation.

Image mosaicing results, i.e., translations, rotations and scale changes between each couple of consecutive images, were finally used for correctly assigning the line acquired with the spectrometer within the investigated area. This made it possible the construction of the images of the area under investigation at the different wavelengths, i.e., the hyperspectral cube.

4. The case study

A proximal sensing field survey was conducted in San Teodoro (Sardinia) with the spectrometer platform mounted on an ultralight airplane. The aim of the survey was to demonstrate the suitability of the hyperspectral device to highlight the presence of vegetation. With respect to [17], this contribution investigates a different area where due to the heterogeneous land cover, the detection of vegetation may be challenging. A further novelty respect to [17] lies in the use of the vegetation indices to verify if they are suitable to highlight vegetated areas. Both the visual check of the map of the area under investigation (i.e., the map provided by Google Earth) and the comparison with the results of the classification procedure will be used to check results.

Roughly 400 images were acquired with the frame rate of both the spectrometer and mosaicing cameras set to 25 fps. The mosaic and the hyperspectral cube images output by the mosaicing procedure were geo-referenced within the WGS-84 geographic coordinate system datum, with ground control points selected using a georeferenced map of the area (e.g., a map obtained from Google Earth) (Fig. 2 and Fig. 3). Control points are landmarks found on both images like road intersection and natural features. In [17], we conducted an accurate analysis of the errors associated to the mosaicing and georeferencing procedure. Applying the georeferencing procedure four times using 7, 10, 15 and 20 points, the mean deviation varied between 3.76 and 3.47 (3.61 on average) pixels. Given that one pixel in the Google map is equal to approximately 0.57 m, the deviation varies between 2.14 and 1.94 m. In [17], we also showed that changes due to an increase in the number of points employed for the georeferencing operation appear negligible, indicating that the distribution of the points is more important than the number of points.

In Fig. 4, the hyperspectral cube of the area under investigation, built with 61 images ranging from wavelengths of 400 nm to 1,000 nm with a step of 10 nm, is displayed in RGB using images at the 660 nm (R), 560 nm (G) and 480 nm (B) bands. The signature of emerging rocks was employed for the radiometric calibration of the hyperspectral cube.

To identify vegetated areas, the Spectral Angle Mapper classifier was employed. The classifier determines the spectral similarity between two spectra by calculating the angle between the spectra and treating them as vectors in a space with dimensionality equal to the number of bands. The maximum angle threshold used was 0.15 radians. In Fig. 5 the result of the classification procedure is presented as well as the average spectral signature of the vegetated areas obtained from the classified hyperspectral cube. The vegetated surfaces indicated by the classifier, highlighted as yellow hatched filled areas, correspond very well to the vegetation identifiable in the map of the area under investigation (Fig. 2). The vegetation spectral signature presents the typical features previously described, i.e., green peak, chlorophyll wells, red edge and NIR plateau.

Moreover, a few vegetation indices were employed as an additional tool i) to transform hyperspectral data into a single image band representing the vegetation distribution and ii) to test the possibility of using VIs to highlight vegetated areas and the vegetation health state. With respect to [9] and [10], we focus on fewer indices, i.e., the broadband indices, because they are more consolidated than narrowband indices due to their recurrence in the literature. In Table 1 the list of VIs used in this study is provided. ρ refers to reflectance and the subscripts refer to specific spectral bands or wavelengths (i.e., NIR refers to the average in the band interval 750–1,100 nm, RED to the average in the band interval 600–700 nm and GREEN to the average in the band interval 500–600 nm).

Fig. 6 presents the map of Red NDVI for the area under investigation and demonstrates the potentiality of the vegetation index to identify vegetated areas. Red NDVI was chosen for its recurrence in the literature. Pixels with a high value of Red NDVI, associated with the color green, correspond very well to vegetation identifiable in the map of the area under investigation (Fig. 2).

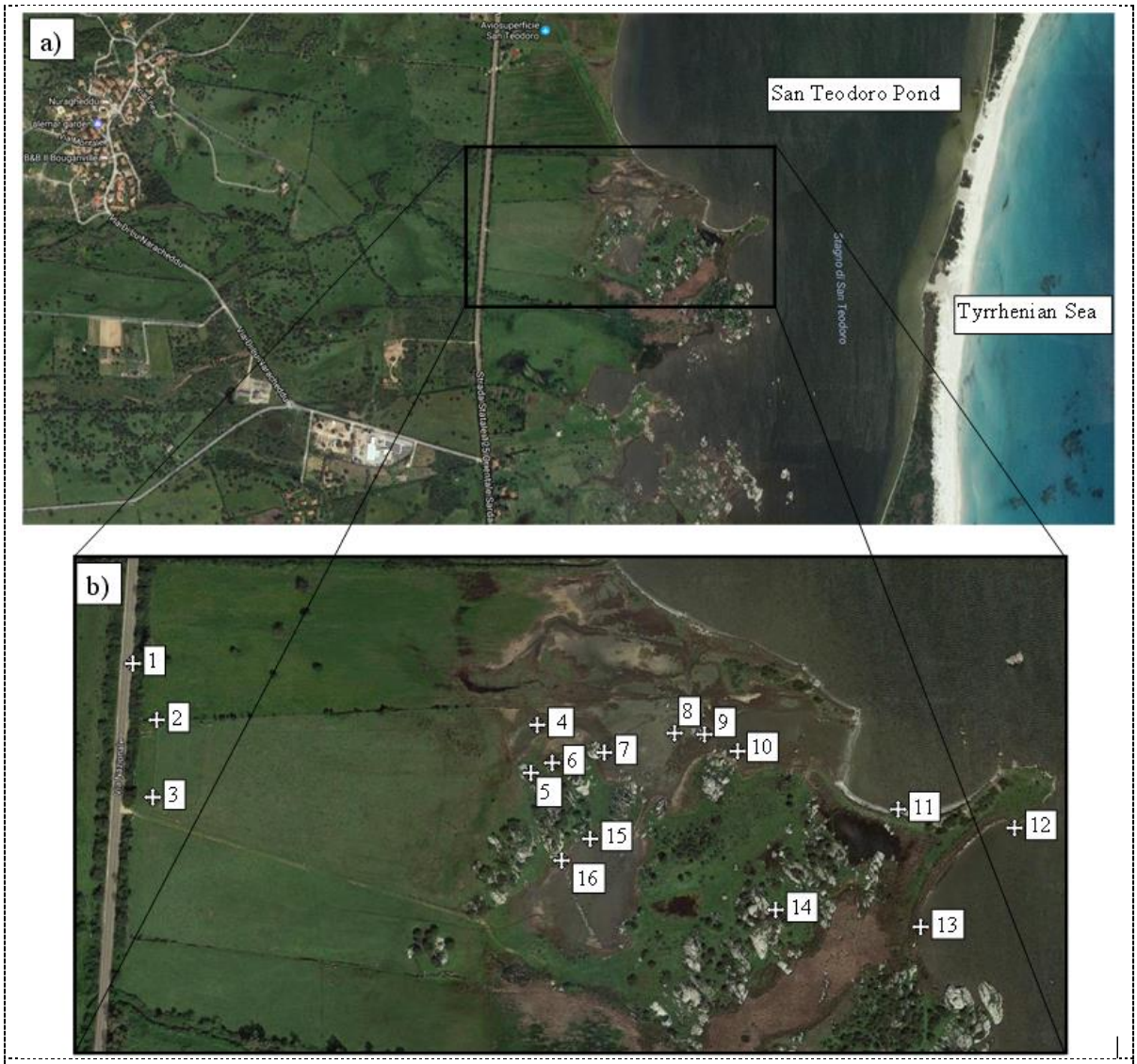

Figure 2. a) Area of interest (San Teodoro ponds); b) zoom in the area monitored with the hyperspectral platform (from Google Earth). The points employed for the geometric transformation are shown in the map**.**

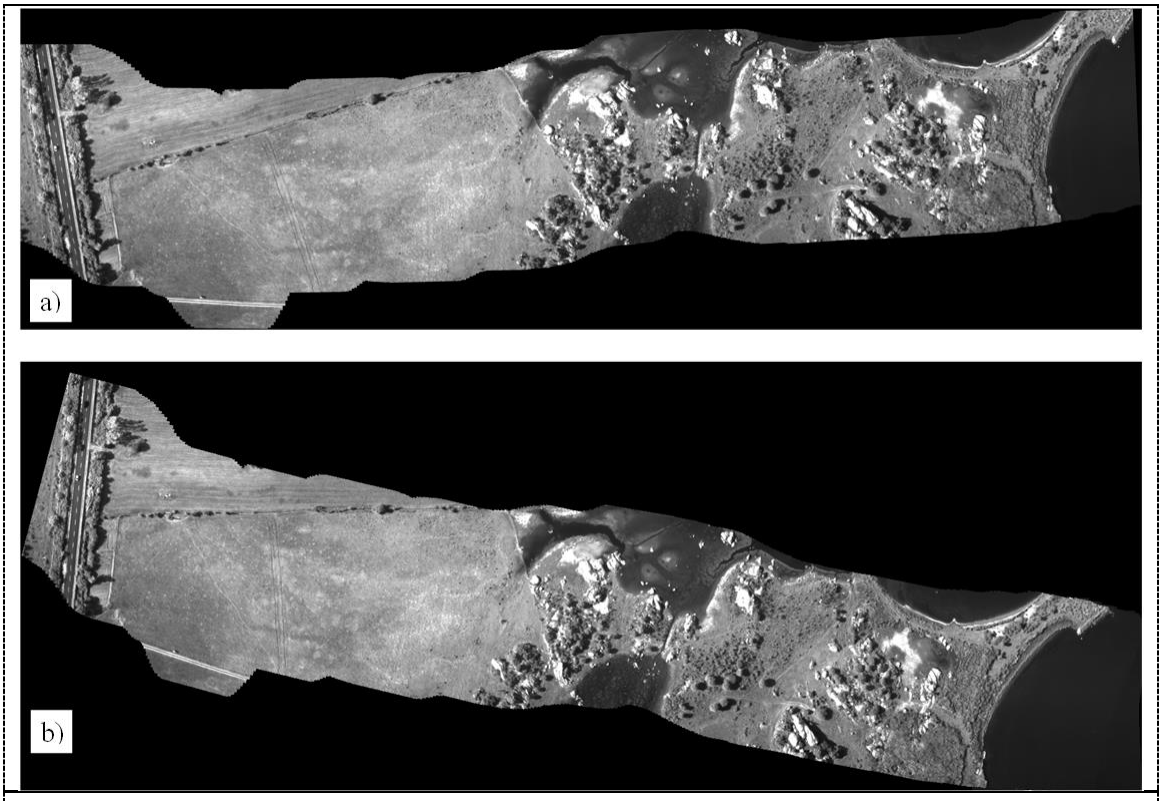

Figure 3. Result of the mosaicing procedure applied to 380 images acquired with the camera Dalsa 4M60 equipped with a standard lens. a) Mosaic before the geo-referencing procedure within the WGS-84 geographic coordinate system datum; b) Georeferenced map.

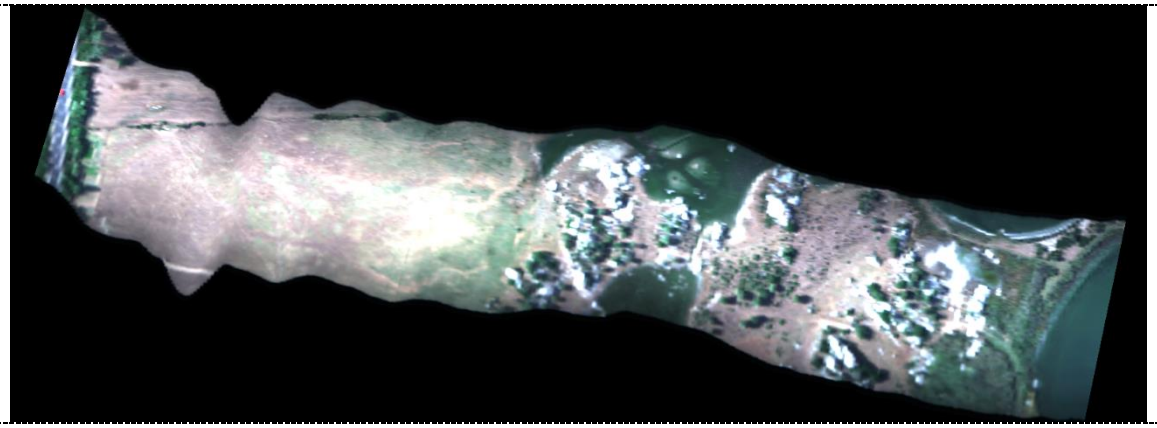

Figure 4. Hyperspectral cube representation in RGB using images at bands 660 nm (R), 560 nm (G) and 480 nm (B).

The broadband indices Red DVI, SR and TVI were employed as well. They provided similar vegetation maps which, for this reason, were not included in the manuscript. Using the results of the classification procedure as the reference, the percentage of vegetation identified by each index respect to the total vegetation coverage was computed. Among the VIs investigated, TVI performs better than the other ones with 99% of vegetation properly identified. For the other indices, over 97% of vegetation is recognized.

Table 1. Vegetation indices investigated.

Vegetation indices		Equation
Red Difference Vegetation Index	Red DVI	$\rho_{NIR} - \rho_{red}$
Simple Ratio	SR	ρ_{NIR} / ρ_{red}
Red Normalized Difference Vegetation Index	Red NDVI	$(\rho_{NIR} - \rho_{Red}) / (\rho_{NIR} + \rho_{Red})$
Triangular Vegetation Index	TVI	$0.5(120(\rho_{NIR} - \rho_{green}) - 200(\rho_{NIR} + \rho_{green}))$

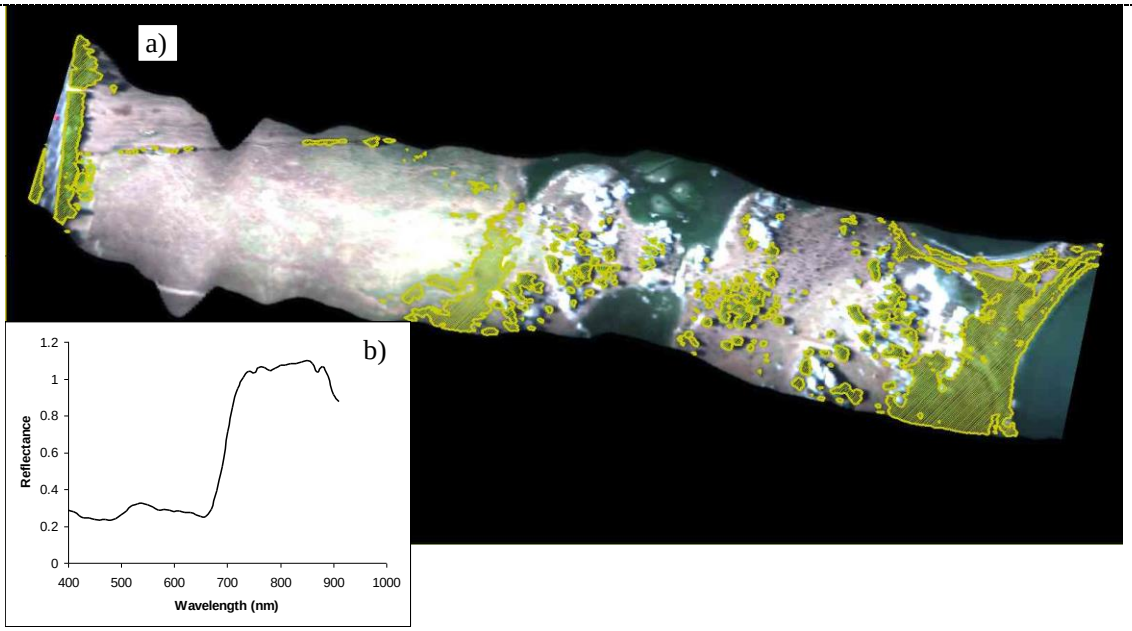

Figure 5. a) Map of the investigated area with vegetated areas identified with the classification procedure highlighted and b) spectral signature of the vegetated area.

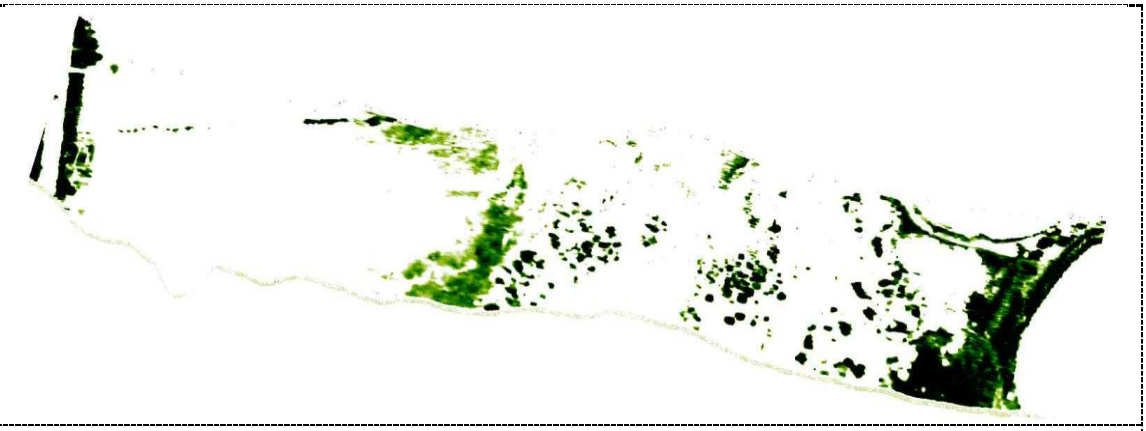

Figure 6. Map of Red NDVI highlighting vegetated areas.

5. Conclusions

The results of the monitoring field survey conducted in San Teodoro (Sardinia) described here have

helped the design and setup of the push-broom hyperspectral sensing device. The hyperspectral platforms provide high spectral resolution (10 nm) and remarkable spatial resolution on the order of a few centimeters, allowing a great detail of information to be extracted.

The computation of vegetation indices turns out to be a fast and efficient way to manage the huge amount of data provided by the sensing devices. The computation of Red DVI, SR, TVI and Red NDVI allowed the transformation of a n-layer hyperspectral cube into a single image band which well represents the vegetation distribution. Nevertheless, no attempt is made to correlate the value assumed by the indices to the vegetation health state due a lack of proper control data on the ground. The procedure was limited to the computation of the above-mentioned VIs but no reasons prevent us from generalizing the procedure and computing other vegetation indices. In this contribution, the vegetation detection was conducted employing broadband indices. Nevertheless, the hyperspectral sensors provide high spectral resolution data that may be profitably employed to compute narrowband indices that are likely to be more effective to characterize the vegetation.

References

[1] Sims AD and Gamon JA 2002 *Remote Sensing of Environment* **81** 337-354.
[2] Zarco-Tejada P.J., Morales A, Testi L and Villalobos FJ 2013 *Remote Sensing of Environment* **133** 102–115.
[3] Gowen A, Tsuchisaka Y, O'Donnell C and Tsenkova R 2011 *American Journal of Analytical Chemistry* **2**(8) 53-62.
[4] Ollinger SV 2011 *New Phytol.* **189** 375–394.
[5] Anderson K and Gaston KJ *Frontiers in Ecology and the Environment*, **11**(3) 138–146.
[6] Li L, Zhang Q and Huang D 2014 *Sensors* **14** 20078–20111.
[7] Thenkabail PS, Smith RB and De-Pauw E 2002 *Photogramm. Eng. Remote Sens.* **68** 607–621.
[8] Gilabert MA, Gonzalez-Piqueras J, Garcia-Haro FJ and Melia J 2002 *Remote Sensing of Environment* **82** 303310.
[9] Agapiou A, Hadjimitsis DG and Alexakis DD 2012 *Remote Sens.*, **4** 3892-3919.
[10] Xue J and Su B 2017 *Journal of Sensors* ID 1353691.
[11] Broge NH and Mortensen JV 2002 *Remote Sensing of Environment* **81** 45 47.
[12] Kaneko K and Nohara S 2014 *Journal of Geographic Information System* **6** 733-742.
[13] Feng Q, Liu J and Gong J 2015 *Remote Sens.* **7** 1074-1094.
[14] Stanton C, Starek MJ, Elliott N, Brewer M, Maeda MM and Chu T 2017 *Journal of Applied Remote Sensing* **11**(2) 026035.
[15] Lucieer A, Malenovsky ZK, Veness T and Wallace L 2014 *Journal of Field Robotics* **31**(4) 493–727.
[16] Capel D 2004 *Image Mosaicing and Super-resolution*. In Distinguished Dissertations, Springer-Verlag London, 47-79.
[17] Moroni M, Dacquino C and Cenedese 2012 *Sensors* **12** 10228-10247.